SOME HEAT-RESISTANT PROPERTIES OF COMPOSITE STRUCTURES AND COATINGS BASED ON REFRACTORY METALS AND ALLOYS OF SOLID-PHASE PREPARATION

Valery P. Korzhov, Vyacheslav M. Kiyko

Institute of Solid State Physics, Russian Academy of Sciences,
Chernogolovka, Moscow region, 142432, Russia

Abstract

The microstructure and mechanical properties of layered type composite materials based on niobium and molybdenum, intended for use at high temperatures, are investigated. Developed materials should ideally have a multi-layer structure of hardening and visco-plastic layers. As strengthening phases, intermetallic compounds based on niobium and molybdenum with silicon and boron or carbon and boron were used. Visco-plastic layers are alloys based on the same niobium and molybdenum. In this work, multicomponent niobium alloys have also been tested. A distinctive and significant feature of the developed laminates is the use of solid-phase "technology" to produce a layered composite using diffusion welding under pressure of artificially assembled packets. For example, for composites with strengthening boridosilicides of niobium or molybdenum, the packets were assembled from thin Nb- or Mo-ribbons with (B–Si)-coatings. For the production of packets with multicomponent niobium alloys, the packet was assembled from Nb-foils with a powder multicomponent coating. Formation of reinforcing layers and alloys occurred simultaneously in the process of welding the package. A pilot experiment was performed to test the possibility of obtaining a heat-resistant coating of tungsten compounds on the surface of the package along with its diffusion welding.

Keywords: *layered composite, niobium alloy, molybdenum, heat-resistant coating, boridosilicide, carbidosilicide, diffusion welding, solid-phase interaction*

1. INTRODUCTION

The development of structural materials intended for use at high temperatures, based on niobium and molybdenum, in particular using the latter, can lead to the production of materials with the highest operating temperature ceiling.

A high modulus of elasticity in molybdenum and its intermetallic compounds suggests that materials based on them can achieve high strength and rigidity (Kosolapova, TYu 1986; Schneibëel, JH 2003; Sharif, AA 2005). In addition, high melting points, high-temperature strength and creep resistance of these compounds, as well as the possibility of organizing increased resistance to oxidation, such as Mo-Si-B alloys (Jain, P 2010), open up a real prospect of obtaining heat-resistant materials, including composite ones, on their basis.

The combination of molybdenum and its intermetallic compounds in the structure of the composite material also makes it possible to reduce the density of such a composite in comparison with the density of molybdenum proper due to the relatively low density of borides and silicides of molybdenum (Goronovsky, IT 1987).

The problem of crack resistance of a composite, which exists in connection with the presence of brittle compounds in the structure of the material, is not insurmountable. One of the possibilities of solving it by slowing the crack at the weak interface of fragile phases was first shown in 1964 in J. Cook and J.E. Gordon (Cook, J 1964). This idea was subsequently used in the development of various layered and fibrous composite materials (Anishenkov, VM 1978; Kolchin, AA 2001). Proceeding from what has been said, it can be expected that the optimal organization of a layered structure with alternating layers of intermetallic compounds and relatively plastic layers of solid solutions of boron and silicon in molybdenum with the corresponding characteristics of the interfaces between phases will be able to provide an acceptable for the structural material level of crack resistance.

The production of structural elements from composite materials in many cases takes place at the stage of formation of the structure of the material, and not after its production due to the complexity of processing such materials after the completion of the formation of their structure in the technological process. In addition, the combination of technologies for obtaining the material and the structural element makes the entire process cheaper.

However, in a number of cases, the shaping of a finished product to a composite material presents a challenge. The proposed technological scheme for the production of layered composites based on molybdenum and niobium, as well as multicomponent niobium alloys, makes it possible to mold products from them quite simply at the stage preceding the formation of brittle intermetallides, when the structure of the preform does not yet contain them.

2. PACKING CONSTRUCTIONS AND ASSEMBLING, COATING

The initial packets could be assembled by simple overlapping of pieces of metal tapes (foils) with one- or two-sided suspension coatings on top of each other. Suspensions are suspended fine powders in organic liquids. As an organic material used polyvinyl butyral and polyethylene glycol. For the M/(Si–B) and Nb/(Si–B) packets, suspensions were used from a mixture of silicon and boron powders with a Si/B ratio of 3 in polyvinyl butyral.

Coatings were applied to the foil by the "staining" method through a metal grid of fine wire (Figure 1). The uniformity of the coating thickness over the entire area of the individual foil was controlled by the diameter of the wire mesh. The thickness of the coating in different packets was varied using wire meshes with different diameters. Before assembling the packages, the coatings were dried at 150–180 °C in a drying cabinet (if polyethylene glycol) or at room temperature on air (if polyvinyl butyral).

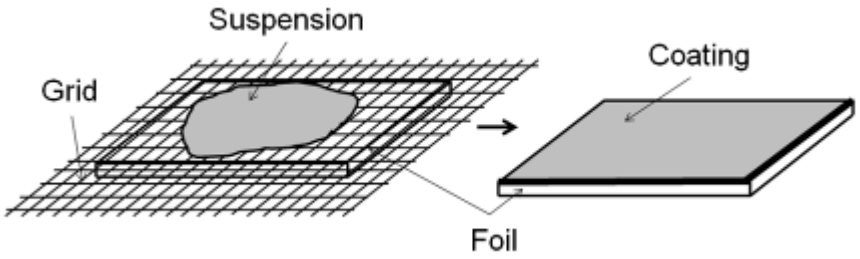


Fig. 1. A simplified scheme for depositing slurry coatings on Nb- or Mo-foils

A more original and compact assembly of multi-layer packages was carried out using elements of the "book" (U-shaped) shape, made of metal foils (Figure 2). As a rule, one-sided coatings were applied to elements prepared beforehand. In some cases, U-shaped elements were prepared from foils with already applied coatings.

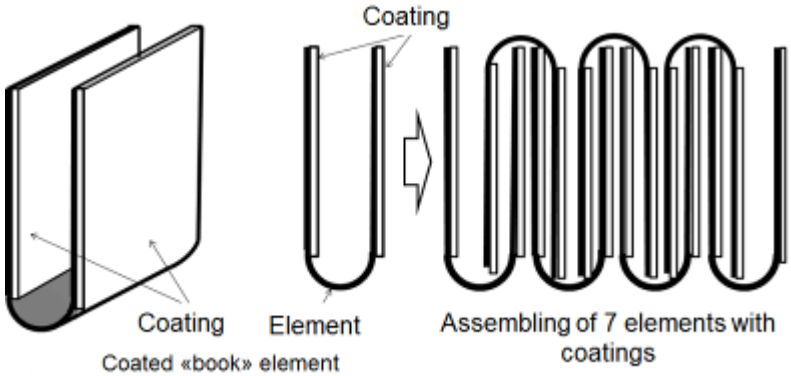


Fig. 2. Assemblage of multi-layer packages from elements of "book form" with one-sided coating on the surfaces of elemental metal foils

One-sided coating for the element means applying it to individual elemental foils on one side of each of them. In this case, one coating is outside the element, the second is inside the element. Then inside the assembled package, the foils alternate with one coating layer (see Figure 2). In the assembled package one of the extreme elements has only an inner covering. Bilateral coating in the elements means that coatings are applied to all four of its surfaces. Then, in the assembled package, the foils are contacted through a double coating layer. The two extreme elements in the package have three covers without one outer.

If the packages from individual foils had to be fastened with thin copper wire so that they did not crumble, then after light pressing using a manual hydraulic press, the packages of the "book" assembly kept "monolithic", allowing them to carry out the necessary operations. Other methods of coating were also tried.

1. A carbide coating was simply applied to pieces of metal tapes as a result of heat treatment (HT) under the pressure of a package made up of metal tapes alternating with two layers of an exfoliated graphite tape of the Graflex brand. After HT, the package was easily disassembled over the contact surfaces of the graphite tapes. The pieces of metal tapes were mechanically cleaned of excessive graphite and dense carbide layers remained on both of their surfaces.
2. The preparation of (Si–C)- or (B–C)-coatings can be carried out by spreading between the metal surface and the graphite tape, respectively, silicon or boron powders, applying their suspension coatings on the surface of the tapes of exfoliated graphite.
3. In a rather large amount, carbon in the form of CO penetrated into the space between the metal foils, on the surface of which the powder coating was applied, during the diffusion welding of the package. This was due to the fact that the heating in the chamber was carried out by a graphite heater.

Thus, before the diffusion welding, the of tapes were alternating metallic layers (of niobium or molybdenum) and coating. The width and length of the pieces of metal tapes were of the order of 30-40 and 50-70 *mm*, respectively. In each package, the rolling direction of all foils was oriented along its length or width.

3. METHODS FOR STUDYING THE STRUCTURE AND IDENTIFICATION OF PHASES

Microstructural studies involving the imaging of objects in secondary and backscattered electrons and X-ray spectral analysis (XSA) were performed on digital electron scanning microscopes Tescan VEGA-II XMU and CamScan MV230. Both microscopes had W-cathodes and were equipped with secondary and reflected electron detectors and an energy-dispersive X-ray microanalyser. Processing of the characteristic X-ray emission spectra was carried out using the software package The Micro-analysis Suite 18d + SP3 (INCA Suite version 4.15) developed by Oxford Instruments, which is based on the algorithm for introducing matrix corrections PAP (Pouchou, JL 1984). The accelerating voltage is 20 *kV*, the current of the electronic probe is 200 *pA*, the size of the electronic probe is 0.16 μm.

Identification of the detected phases was carried out with the help of local XSA. The spectra belonging to the same phase were grouped and computed the mean values of the concentrations for each of the elements. When establishing the chemical composition of the phases, carbon and boron were not determined, but were calculated "by difference". To establish the probe current, the reference sections of niobium and molybdenum placed in the cage with the samples under investigation were used. However, with a rigorous approach, analysis of these elements should be considered semi-quantitative. We used XSA data to identify the detected phases with known stoichiometric indices and for a relative comparison of the concentrations of carbon and boron in different phases.

4. COMPOSITES HARDENED BY COMPOUNDS OF *MO* OR *NB* WITH *SI* AND *B*

The first multilayer packets of Mo/(Si–B) and Nb/(Si–B) were assembled from thin molybdenum and niobium foils with suspension coatings.

4.1. Composites of Mo/(Si–B)

The content of (Si–B) coatings in Mo composites varied from 4.27 to 7.72 mass%. Packages with molybdenum 1- and 2-Mo/(Si–B) (Table 1) differed in that they were assembled using Mo-foils with one- and two-sided (Si–B) coatings. It would seem that, under the same diffusion welding conditions, they should differ substantially in the contents of the coating. However, the concentrations of silicon and boron in the packages differed insignificantly – 4.27 and 4.69% by weight, respectively, in Mo-packets with one- (2) and two-sided coating (1).

To trace the change in the microstructure as a function of temperature, the 5-Mo/(Si–B) package containing 7.72% by weight of the coating (see Table 1) was first welded under pressure at 1500 °C and then subjected to a thermal treatment at 1700 °C in the "stolen" state. The package is clamped in a high-strength graphite clamp. It was assumed that the main pressure would be created due to the expansion of the composite.

<table>
<tr><td colspan="2">Data on structural elements and modes of diffusion welding (DW)</td></tr>
<tr><td>1-Mo/(Si–B)</td><td>2-Mo/(Si–B)</td></tr>
<tr><td>Mo-foil 50 microns thick – 17 pcs.
2-sided (Si–B)-coating – 16 pcs.
(Si–B)-coatings – 4.69 mass.%.
Packet thickness after DW – 1.10 mm.</td><td>Mo-foil 50 microns thick – 16 pcs.
1-sided (Si–B)-coating – 15 pcs.
(Si–B)-coatings – 4.27 mass.%.
Packet thickness after DW – 0.95 mm.</td></tr>
<tr><td colspan="2">Mode DW: 1500 °C, 30 min at 10.5 MPa (1.5 T) + 30 min at 14.0 MPa (2 T)</td></tr>
<tr><td>3-Nb/(Si–B)</td><td>4-Nb/(Si–B)</td></tr>
<tr><td>Nb-foil 60 microns thick – 22 pcs.
1-sided (Si–B)-coatings – 21 pcs.
Thickness of the packet after DW – 1.7 mm.
DW: 1500 °C, 1 h at 14.0 MPa (2 T).</td><td>"Book" elemenst of Nb-foil 60 microns thick – 7 pcs.
<u>Amount:</u> Nb-foils – 14 + 1 = 15 pcs.;
1-sided (Si–B)-coatings – 14 pcs.
<u>Content:</u> (Si–B)-coatings – 15.5 mass.%;
two (Mo–W–Si)-coatings – 7.8 mass.%.
Thickness of the packet after DW – 1,6 mm.
DW: 1500 °C, 1 h at 7.4 MPa + 1500 °C (1 h at 11.8 MPa and 2 h at 15.7 MPa).</td></tr>
<tr><td colspan="2">5-Mo/(Si–B)
"Book" element of Mo-foil 50 microns thick – 15 pcs.
<u>Quantity:</u> Mo-foils in the packet – 30 pcs.; 2-sided (Si–B)-coatings – 29 pcs.
Content of (Si–B)-coatings – 7.72 mass.%.
The thickness of the packet before and after the DW is ~ 8 and 3.2 mm, respectively.
1st stage. DW: 1500 °C, 1 h at 12.4 MPa (30 min) and at 8.3 MPa (30 min).
2 nd stage. Heat treatment of the packet in the clamp from graphite: 1700 °C, 20 min in Ar.</td></tr>
</table>

Table 1. Design and modes of diffusion welding of bags Mo/(Si–B) и Nb/(Si–B)

The macrostructure of the cross sections of both packages after welding consisted of alternating layers of light background associated with the molybdenum layers and diffusion zones of interaction (ZI) of molybdenum with (Si–B)-coating. In Figure 3*a* shows the structure of the Mo/(Si–B) package with 4.27% by weight of the coating after DW at 1500 °C. It can be seen that the layers of ZI are uneven in thickness – from their almost complete absence to ~ 70 *μm*. The nonuniformity in the thickness of the interaction zones was also observed in the packet with 4.69 mass.% coating.

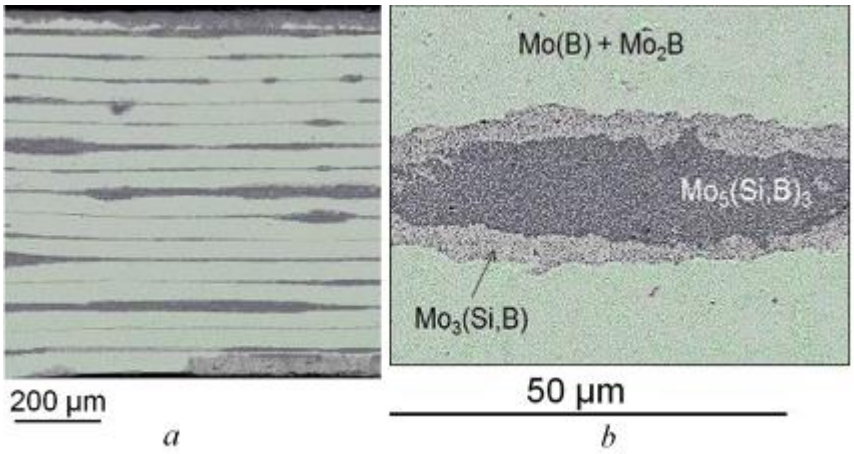


Fig. 3. Composite after DW of package with 4.27 mass.% (Si–B): *a* – cross-sectional structure; b – the microstructure of the interaction zone, Mo(B) is the solid solution of boron in Mo

According to the X-ray spectral analysis in the Mo layers of both composites near and at some distance from the ZI, the boron content varied from 17 to 28 at.%, and silicon was almost not detected. This was observed despite the fact that according to their diagrams of state with molybdenum, at 1500 °C the solubility of boron in molybdenum, although it is, but is very small, and silicon can dissolve up to ~ 2 at.%.

The obtained boron content corresponded to the eutectic Mo(B) + Mo_2B region of the Mo-B state diagram, where Mo(B) is a solid solution of boron in molybdenum, responsible for the visco-plastic behavior of the composites at room temperature. But the microstructure of zones of interaction in both composites differed significantly. Although both packages differed insignificantly with the content of silicon and boron, the phase composition of the microstructure of the ZI of the composites obtained from them was different.

The phase structure of the interaction zone in a composite with a smaller content of the coating is shown in Figure 3*b*. According to local X-ray spectral analysis, the detected phases can be identified by one of two possible variants – either Mo_3(Si,B) and $Mo_5(Si,B)_3$, as shown in the figure, or Mo_2(B,Si) and Mo(B,Si). For the final phase determination, it was also correct to use X-ray structural analysis. But for any of the variants, it can be argued that in this composite the phase structure of the interaction zone is close to an almost completed state, since one of the two identified intermetallic compounds is the maximum molybdenum content of all compounds existing in the Mo–Si and Mo–B state diagrams, respectively. No other compounds were found in this composite.

The interaction zones in the composite obtained from the 4.69 mass% (S–B) package, depending on the thickness, are represented by two types of structure, differing in morphology and phase composition (Figure 4). In the interaction zones of thickness ~ 60 *μm*, two at least 2-phase layers with a gray phase growing in the direction from the middle of the zone perpendicular to the layers, and a middle layer with a large number of pores are distinguished. In ZI of thickness of 20–30 *μm*, the pores were much smaller.

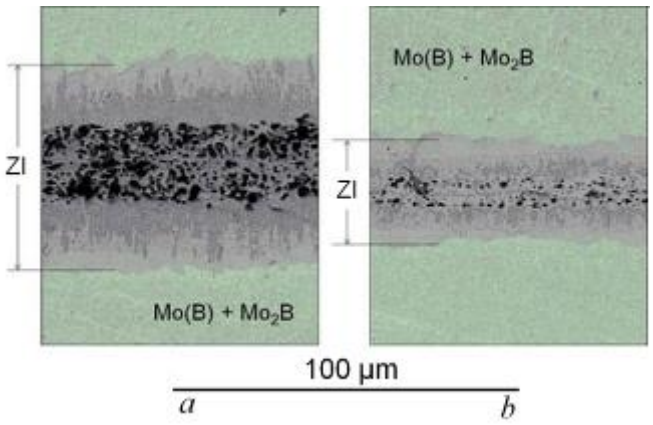


Fig. 4. Microstructure of two types of ZI in the composite after DW of the Mo/(Si–B) c 4.69% (Si–B): Mo(B) is a solid solution of boron in Mo; ZI – zone of interaction

With the help of scanning electron micro-scopy and local XSA, it was established that two layers of the interaction zone in Fig. 4*a*, located between its porous middle and Mo(B) + Mo2B layers, were inhomoge-neous in phase composition. Their extreme 1-phase interlayers of thickness ~10 *μm* (Figure 5), bordering with Mo (B) + Mo_2B, consisted of Mo_2B but in which silicon was dissolved – $Mo_2(B,Si) \equiv Mo_{1,87}(B_{0,99}Si_{0,14})_{1,13}$.

Closer to the middle of the interaction zone, two-phase intermediate layers from the equiatomic compound $Mo(B,Si) \equiv Mo_{1.06}(B_{0.63}Si_{0.31})_{0.94}$ of dark gray contrast and a compound based on molybdenum intermetallide with silicon Mo_5Si_3 having relatively a wide range of homogeneity, $Mo_5(Si,B)_3 \equiv Mo_{4.29}(Si_{2.42}B_{1.29})_{3.71}$ of gray contrast. The first is a solid solution of silicon in αMoB, the second is boron in Mo_5Si_3.

The middle of ZI with a large number of pores consisted of phases – $Mo_5(Si,B)_3$ and Mo(B,Si). The concentrations of silicon and boron in the compounds in the direction from the periphery of the porous layer to its center varied in favor of boron. In $Mo_5(Si,B)_3$ – from 35.0Si and 3.4 at.%B to 23.1Si and 14.4 at.%B or from $Mo_{4.93}(Si_{2.80}B_{0.27})_{3.07}$ to $Mo_{5.00}(Si_{1.85}B_{1.15})_{3.00}$. In Mo(B,Si) – from 37.9B and 19.2 at.%Si to 57.8 at.%B or from $Mo_{0.86}(B_{0.76}Si_{0.38})_{1.14}$ to the $Mo_{0.84}B_{1,16}$ boride, which dissolved only 0.13 at.%Si. That is, boron was concentrated in the middle region of the porous interlayer of the interaction zone.

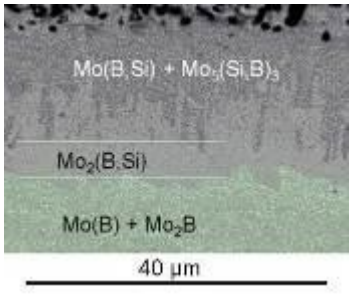


Fig. 5. Microstructure of the fragment of the ZI between its middle layer and the Mo(B) + Mo_2B layer, which was before the DW Mo-foil

An analogous phase composition was observed in a ZI of thickness 20–30 *μm* (Figure 4*b*). Its interlayers bordering Mo(B) + Mo_2B consisted of boride-silicide $Mo_2(B,Si)$, but silicon contained much less than in similar interlayers of the ZI with a porous middle. The middle layer consisted of $Mo(B,Si) \equiv Mo_{1.07}(B_{0.52}Si_{0.41})_{0.93}$ and $Mo_5(Si,B)_3 \equiv Mo_{4.26}(Si_{2.19}B_{1.55})_{3.7}$ compounds. In contrast to the zone of interaction with the porous medium, the distribution of boron over the volume of the zone here was more uniform.

Comparing the two zones of interaction of Mo-foils with (Si–B)-coatings, it can be concluded that the phase structure of the 20–30-*μm* zone was closer to the structural state corresponding to a temperature

of 1500 °C than the ZI with a thickness of 50–60 *μm*. The different thickness of the ZI is due to the heterogeneity of the thickness of the coatings, applied over the still not worked-through methods. To increase the amount of high-temperature phases of boron and silicon with molybdenum can be achieved by increasing the content (Si–B)-coating in the original package. In order to establish its content close to the limiting value, at which the composite does not become brittle after the DW, a composite sample of Mo-foils with a 2-sided (Si–B)-coating was produced, which in the initial package contained 7.72 mass.%.

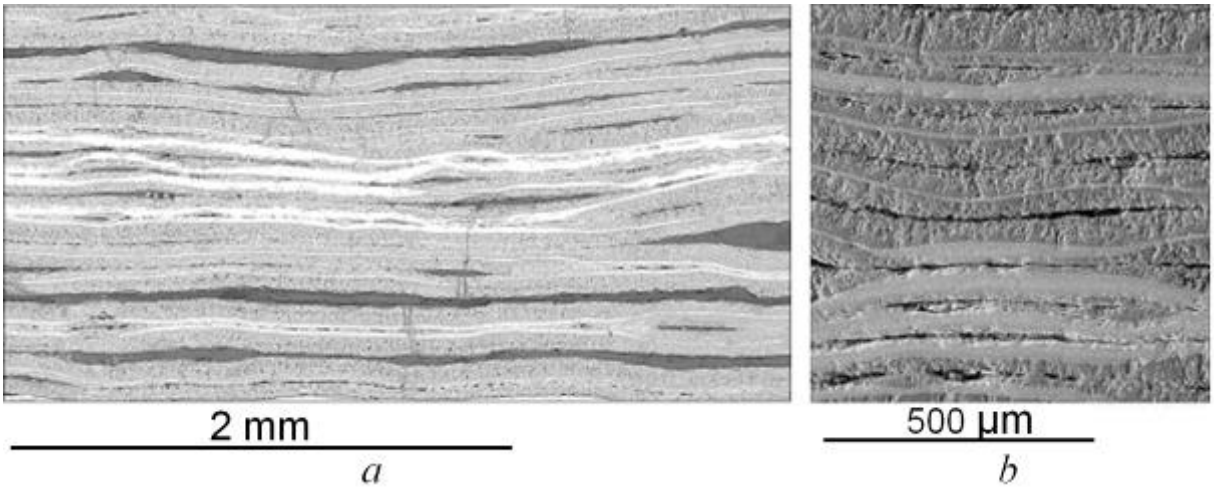


Fig. 6. Macro- (*a*) and microstructure (*b*) of the 5-Mo/(Si–B) composite after DW under pressure at 1500 °C for 1 *h*

Judging from the cross-sectional structure of such a Mo/(Si–B)-composite (Figure 6), the interaction zones in it are present in excess. They correspond to the gray layers. Light layers associated with molybdenum foils occur in a much smaller amount.

As expected, the phase structure of the interaction zones of the composite (Figure 7) was far from complete, since it was characterized by the presence of chemical compounds with the limiting concentrations of B and Si for the Mo–B and Mo–Si systems – Mo_2B_5, MoB_4 and $MoSi_2$.

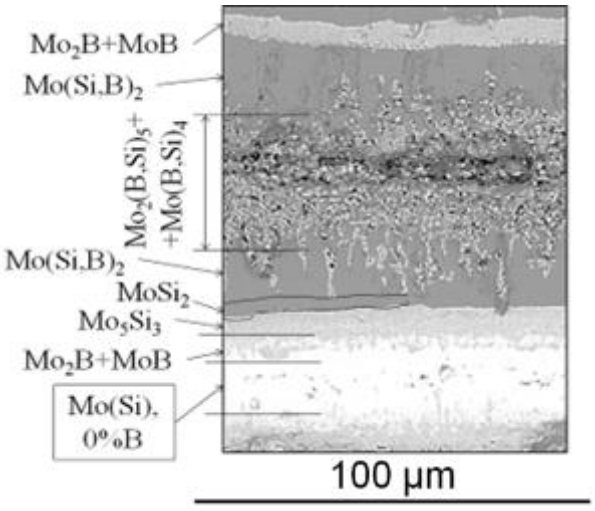


Fig. 7. The microstructure of the composite ZI after the DW of the 5-Mo/(Si–B)-package with 7.72 wt.%: Mo(Si) is a solid solution of silicon in molybdenum

According to the data of the local XSA, the matrix phase of the ZI, which gives the gray-gray background, was identified as a silicide $Mo(Si,B)_2$ with redistribution of silicon and boron in favor of the latter: $Mo_{1.06}(Si_{1.93}B_{0.01})_{1.94}$ (in the boundary interlayer with a light 2-phase layer), $Mo_{0.93}(Si_{1.72}B_{0.36})_{2.08}$ (at a distance of ~20 *μm* from the boundary of the light layer) and

$Mo_{0.90}(Si_{1,50}B_{0.60})_{2.10}$ (near the middle of ZI). Thus, with the approach to the middle of the diffusion interaction zone, the boron concentration in the intermetallide $MoSi_2$ increased from ~0.2 to 19.9 ± 2.0 at.%.

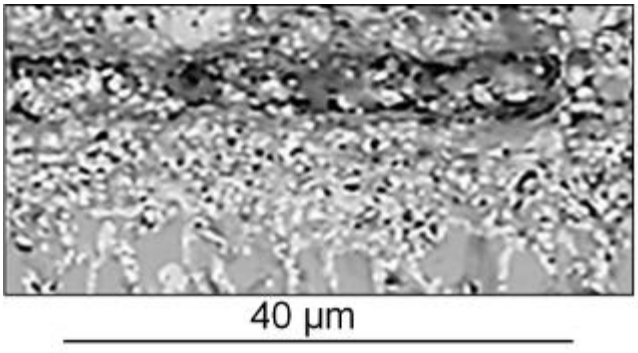


Fig. 8. The microstructure of the middle of the interaction zone in Fig. 7th

On a gray background of the matrix compound $Mo(Si,B)_2$, light precipitates of the approximate composition $Mo_{27.6}B_{71.6}Si_{0.8}$ (at.%) are present in large amounts, which have black inclusions (Figure 8). The composition of the precipitates corresponds to the intermetallic compound $Mo_2(B,Si)_5$. As you move toward the border with light layers, which were previously Mo-foils, these excretions form stitches perpendicular to the layers. In the middle of the zone, dark inclusions were detected identified with a solid solution of silicon in boride MoB_4: $Mo(B,Si)_4 \equiv Mo_{1.03}(B_{2.09}Si_{1.88})_{3.97}$.

Finally, consider the light background layers that have retained molybdenum as the main component. In most cases, they were not thicker than 5–7 μm, almost consuming their "molybdenum potential," with the eutectic composition Mo_2B + MoB.

Significantly less often, their thickness was 40–45 μm. Several such layers occupy the middle region of Figure 6*a*. Their microstructure is shown in the lower part of Figure 7. The middle of thick light layers with a thickness of about 30 μm was a solid solution of silicon in molybdenum Mo(Si). The silicon concentration was not more than 0.25 at.%, and boron was completely absent (Figure 9). But in the layers of these same interlayers located closer to the neighboring diffusion zone, but not yet bordering it, the boron content increased to 42.3 ± 5.00 at.%, and the silicon content remained at the same level of several tenths of a percent. According to the Mo–B state diagram, the composition of the interlayers corresponded to the eutectic region of Mo_2B + MoB. By the way, the same composition was also determined in thin light layers (see the upper part of Figure 7).

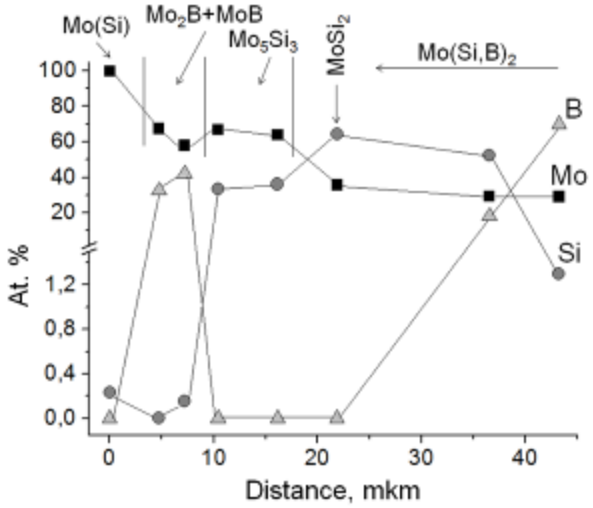


Fig. 9. The profiles of the Mo, Si, and B concentrations of the light layer and the boundary region of the ZI in composite after the DW of the 5-Mo/(Si–B) package with 7.72 mass% (compare with Fig. 7)

But the interlayers in thick light layers bordering with the interaction zone did not contain boron, having the composition $Mo_{65.3}Si_{34.7}B_{0.0}$, corresponding to the compound Si and Mo: $Mo_5Si_3 \equiv Mo_{5.22}Si_{2.78}$.

The sharply nonmonotonic concentration dependence of boron at the boundary of the layer with Mo-solid solution and the interaction zone is apparently due to the formation of an interlayer from the intermetallic compound Mo_5Si_3, through which boron diffusion is too difficult. A prerequisite for this may be the absence of a chemical compound of molybdenum and boron with the same stoichiometry. The boron, which, despite the much lower solubility in molybdenum than silicon, having good atomic mobility, apparently before the formation of Mo_5Si_3, had accumulated in a sufficient amount in molybdenum foils to form a eutectic structure of Mo_2B + Mo(B). Silicon at the same time continued to increase the intermetallide Mo_5Si_3. A thin interlayer in the ZI, which borders with the bright layer through $MoSi_3$, is represented by a matrix silicide $MoSi_2$ with a molybdenum concentration lower than in Mo_5Si_3, and also containing no boron (see Figure 8).

The structure of the composite is determined primarily by the temperature at which mutual diffusion occurs between the foil and the coating.

The investigated composite was subjected to the second stage of thermal processing in argon, consisting of heating to 1700 °C and holding at this temperature for 20 minutes, being clamped in a clamp of high-strength graphite. It was believed that additional pressure on the flat composite sample was created due to its thermal expansion. The structure of the obtained composite (Figure 10) had a clearly pronounced layered character and consisted of only two phases: of the light phase – a solid solution of silicon in boride MoB = $Mo_{0.91}(B_{1.06}Si_{0.03})_{1.09}$ and a phase of dark gray color – a solid solution of boron in a silicide $MoSi_2$ = $Mo_{0.90}(Si_{1.76}B_{0.34})_{2.10}$.

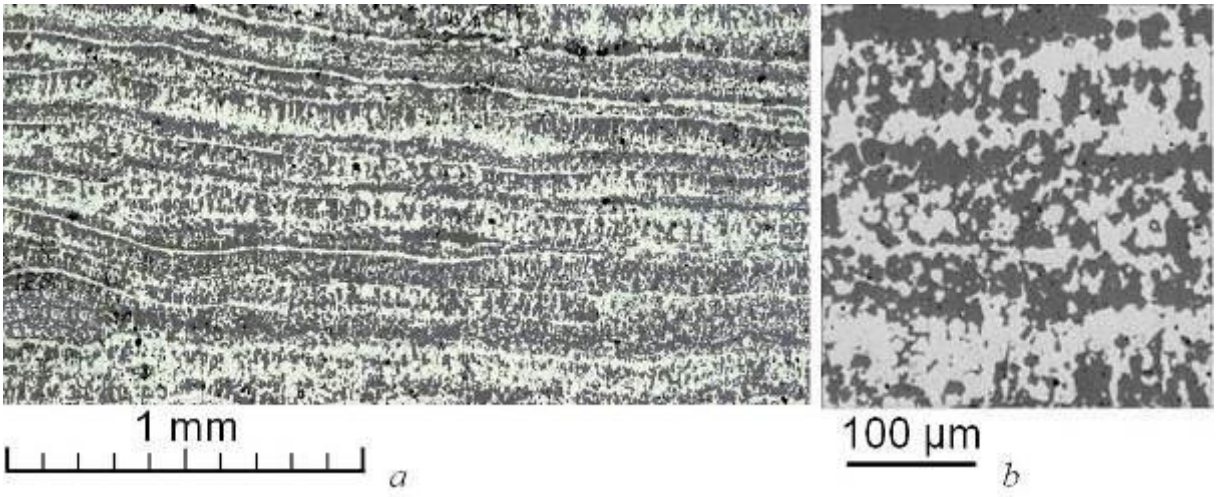


Fig. 10. Macro- (*a*) and microstructure (*b*) of the 5-Mo/(Si-B) composite after the 2nd heat treatment step at 1700 °C in a graphite clamp

As expected, at room temperature, the samples of this composite showed a fragile character of failure, since there was no viscous-plastic eutectic structure in its volume.

The change in the phase structure of composites subjected to welding at 1500 °C, depending on the content (Si–B)-coating in the original package, can be traced and tabulated 2.

	4,27 mass.%	4,69 mass.%	7,72 mass.%
«Mo-layer»	Mo(B) + Mo_2B	Mo(B) + Mo_2B	MoB + Mo_2B in a layer with thickness of ~10 μm; Mo_5Si_3+[Mo_2B+MoB]+Mo(Si) in a layer with thickness ~40 μm
ZI	$Mo_5(Si,B)_3$ + + $Mo_3(Si,B)$	$Mo_2(B,Si)$ and Mo(B,Si)+$Mo_5(Si,B)_3$	$Mo(Si,B)_2$ and $Mo_2(B,Si)_5$+$Mo(B,Si)_4$

Table 2. Phase structure of composites after DW of initial packets with different contents (Si–B)-coatings at 1500 °C

With an increase in the coating content of the silicon-boron powder mixture with the Si/B ratio of 3 for composite layers formed on the site of Mo foils, the "consumption" of the Mo-solid solution was typical. In composites welded from packages with 4.27 and 4.69 mass% coating, layers associated with molybdenum foils contained ~ 22.5 at.% B. This corresponds to the eutectic region of the Mo–B diagram with a phase composition from the viscous-plastic solid solution Mo(B), responsible in the composite for fracture toughness, and the Mo_2B compound. A composite of 7.72% by weight of the coating differed in that a significant proportion of the layers that had Mo-foils and which had a smaller thickness (see Table 2) had boron and molybdenum concentrations corresponding to the eutectic region of the diagram Mo–B with a phase composition of intermetallides Mo_2B and MoB. The creep-prone phase, a solid solution of silicon in molybdenum Mo(Si), was contained in layers of thickness about 40 μm, but there were very few of them in the composite. When the content of the (Si–B)-coating is increased, the phase composition of the interaction zones changes in favor of molybdenum intermetallides with large concentrations of Si and B: $Mo_5(Si,B)_3$ и $Mo_3(Si,B)$ → $Mo(Si,B)_2$, $Mo_2(B,Si)_5$ и $Mo(B,Si)_4$.

4.2. Composites of Nb/(Si–B)

Two types of niobium-based composites reinforced by its compounds with silicon and boron were studied (see Table 1). The first of these was prepared at 1500 °C for 1 hour from a multilayer stack collected by simply applying 60 μm thick Nb-foils with a one-sided (Si–B)-coating. The second composite differed from the first in that the bag was assembled with U-shaped elements of Nb-foils with one-sided coating and the total welding time was 4 hours. In addition, the composite had a coating of intermetallic compounds Mo and W with silicon and carbon, formed simultaneously and in conjunction with its structure in the process of diffusion welding of the package.

Compared with the first Mo-composites, Nb-based composites made from 3-Nb/(Si–B) packs had properly organized layered structures (Figure 11) from the interaction zones of locally generated (Si–B)-coatings that occupy not less than 30–40% of the cross-sectional area, and the bright layers of Nb-solid solution (Nb). According to the diagrams of the Nb–Si and N–B states, the solubility of silicon and boron in niobium did not exceed a tenth of a percent. If they were found, their concentrations were at the sensitivity limit of the XS-analysis.

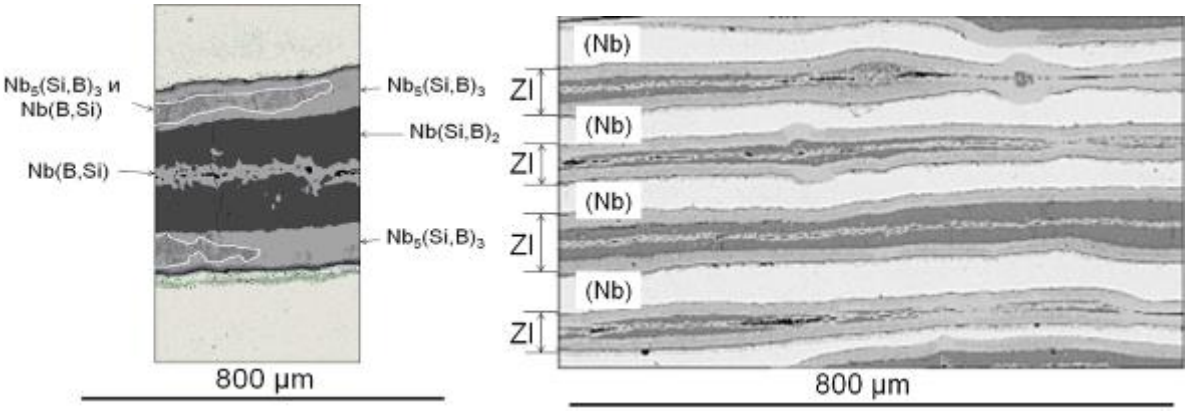


Fig. 11. Microstructure of a cross-section of a composite made from a 3-Nb/(Si–B)-package: (Nb) – Nb-solid solution, ZI – zone of interaction

Fig. 12. The microstructure of the composite ZI after the DW of the 3-Nb/(Si–B) packet assembled by Nb-foils with coatings: time DW – 1 *h*

The outer layers of the interaction zones bordering the niobium solid solution (Nb) had the intermetallic compound $Nb_5(Si,B)_3$ as the main (or matrix) phase (Figure 12). But in these same layers extensive regions with inclusions of dark gray contrast of the intermetallic Nb(B,Si) were observed. Here and in Figure 13*a*, these regions are marked by light contours.

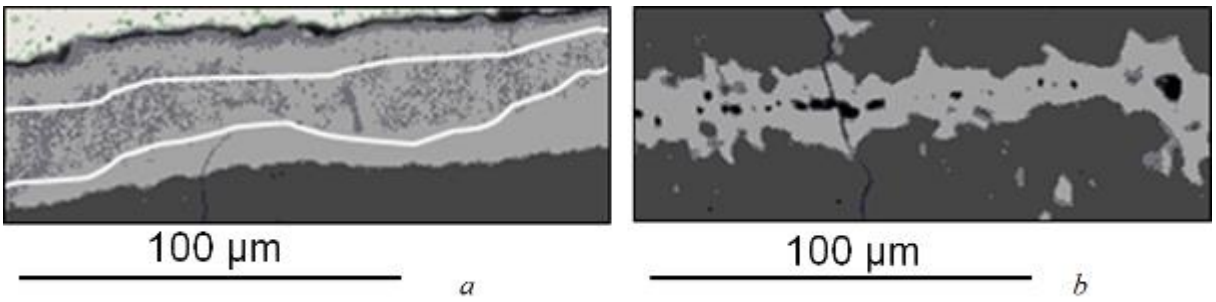


Fig. 13. Fragments of the microstructure in Figure 12 at higher magnification: *a* – a 2-phase region in the outer layer of the ZI; *b* – internal interlayer of ZI

According to X-ray spectral analysis, dark-colored layers were identified with the compound $Nb(Si,B)_2 \equiv Nb_{0.92}(Si_{1.59}B_{0.49})_{2.08}$. The thin layer located in the middle of the interaction zone is related to the equiatomic niobium and boron intermetallic compound $Nb(B,Si) \equiv Nb_{1.01}(B_{0.40}Si_{0.59})_{0.99}$, which exists in the Nb-B diagram, and in the Nb–Si diagram absent. But due to the fact that there is more silicon in the layer than boron, the identification of the layer can be made by using the Nb–Si diagram. The established elemental composition of the layer is in its eutectic region consisting of eutectic (αNb_5Si_3 + $NbSi_2$) and secondary precipitates of the lighter intermetallic $NbSi_2$, which, if detected, should be distinguished by a dark contrast on a light background. It is this picture that can be observed in Figure 13*b*.

The diffusion welding of the second 4-Nb/(Si–B)-packet occurred in two stages at a single temperature of 1500 °C, but at different pressures and for different times.

The first stage of the DW. At the 1st stage, the holding time is 1 hour, the pressure is 7.4 *MPa*. A fragment of the microstructure of the cross section of the composite is shown in Figure 14. Already after holding for 1 hour a significant number of Nb-foils were used almost or completely to form a structure of two layers of the compound $Nb_3(B,Si)_4 \equiv Nb_{2.92}(B_{2.35}Si_{1.73})_{4.08}$ and the "stitch" of porous inclusions, which remained after the coating of (Si–B) (Figure 15).

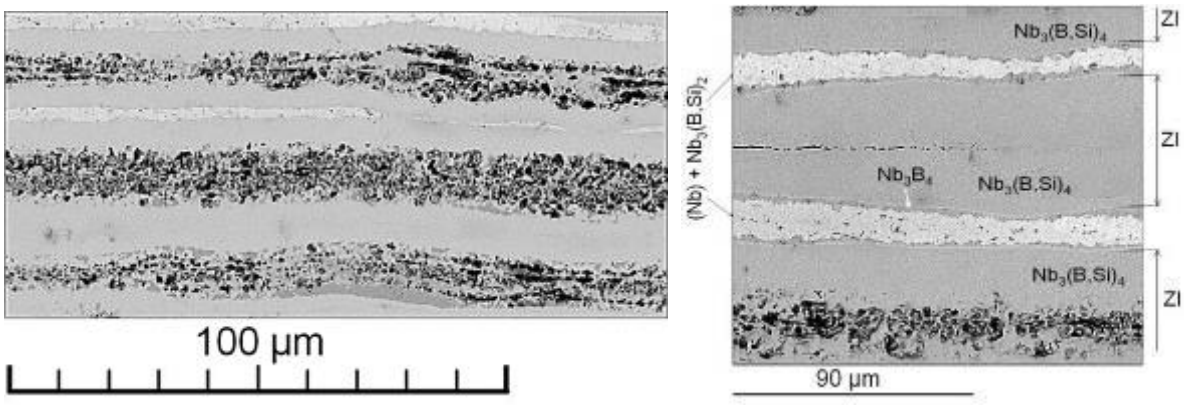


Fig. 14. Layered cross-sectional structure of a niobium-based composite after DW for 1 *h* of a 4-Nb/(Si–B) packet assembled from "book" shape elements

Fig. 15. Phase structure of a characteristic section of the cross-section of an Nb-composite after welding for 1 *h*

Light layers have been preserved by the Nb-foils preserved after welding. The sum of the concentrations of silicon and boron in them was in the eutectic region of the Nb–B diagram with a phase composition of (Nb) and Nb_3B_2, where (Nb) is a solid solution of boron in niobium. Note that these layers were bordered by a thin layer of niobium boride Nb_3B_4.

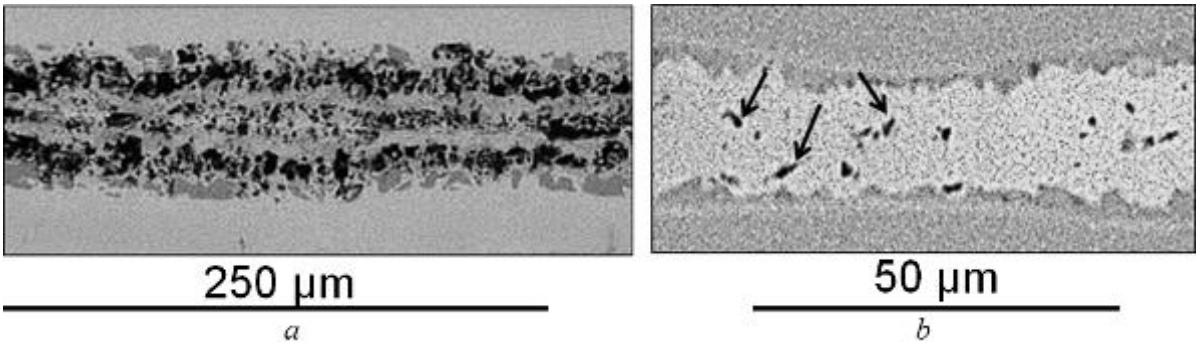


Fig. 16. The phase structure of the cross-section of the 4-Nb/(Si–B) composite after the first stage of the DW (*a*) and the phase structure of its characteristic fragment (*b*)

Another species of ZI, besides two $Nb_3(B,Si)_4$ layers and a line of inclusions (see Figure 15), had a middle of the intermetallic phases (Figure 16*a*) of gray and dark color identified as $Nb(Si,B)_2$ with a small, up to 2 at.%, content of boron and NbB_2 with silicon beyond the sensitivity of the analysis.

The layers that inherited Nb-foils had the composition $Nb_{65,1}(B_{33,2}Si_{1,8})_{35,0}$ (at.%) corresponding to the hypereutectic region (Nb) + $Nb_3(B,Si)_2$ of the triple Nb–B–Si diagram. In addition, $Nb_3(B,Si)_2$ intermetallide was present in the structure of the light layer and in the form of secondary precipitates (Figure 16*b*). A thin interlayer bordering the light layer is Nb_3B_4 boride, but with a very low silicon content $Nb_{43.0}(B_{56.6}Si_{0.4})_{57.0} \equiv Nb_{3.01}(B_{3.96}Si_{0.03})_{3.99}$.

The second stage of the DW. The macrostructure of the 4-Nb/(S–B) composite of niobium after the second stage of the DW, differing from the first by a longer exposure time and twice the pressure, is shown in Figure 17. It can be seen that Nb-foils, which are relatively thin layers of different thickness after welding, are not preserved everywhere. But their full "expenditure" was not associated with an increase in the welding time, because similar cases were often observed after its first stage. It is more likely that this was the result of a thicker suspension coating on this portion of the surface of the Nb tape, in view of the unworked technique for its application.

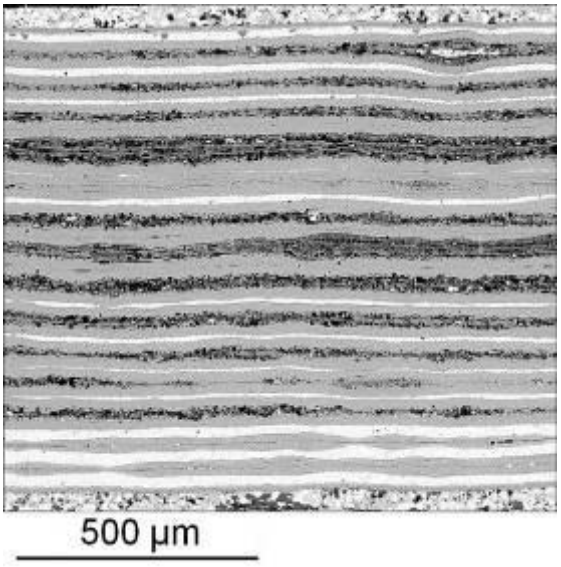


Fig. 17. Macrostructure of the composite after the 2nd stage of the DW: total holding time is 4 hours, pressure is up to 15.7 *MPa*

Another was the phase content of the interaction zones between Nb-foils and coatings (Figure 18). Two of its main layers with a thickness of ~ 40 *μm* are represented by a solid solution of boron in $Nb_5(Si,B)_3$. Its averaged composition is $Nb_{4.97}(Si_{2.87}B_{0.16})_{3.03}$. The middle regions of the ZI contained at least two reliably identified phases. The first is a solid solution of boron in $NbSi_2$: $Nb(Si,B)_2 \equiv Nb_{0.98}(Si_{1.93}B_{0.09})_{2.02}$. The second is a solid solution of silicon in NbB: $Nb(B,Si) \equiv Nb_{0.86}(B_{1.10}Si_{0.03})_{1.14}$.

But the light layers remaining from Nb-foils also had a different content of elements. If, after 1-hour welding, the layer structure was hypereutectic with the boron content prevailing in comparison with silicon, then after 4 hours of welding the layers consisted of niobium, which dissolved only up to 0.4 at.% Si.

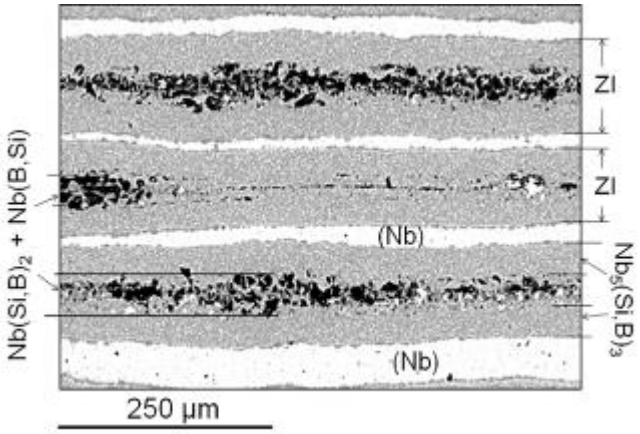


Fig. 18. The microstructure of the composite after the 2nd stage of the DW: the total holding time is 4 hours, the pressure is up to 15.7 *MPa*

In Figure 19 presents a detailed analysis of the phase components in the composite structure after the second DW.

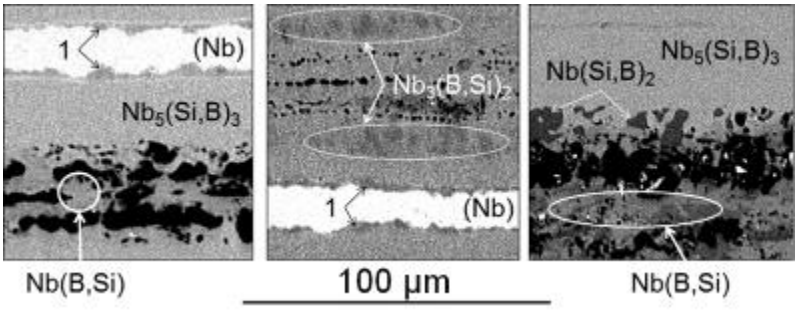


Fig. 19. Three characteristic fragments of the microstructure of the cross-section of the 4-Nb/(Si–B) composite after the second stage of the DW. The phases were identified by local XS analysis

1. Interlayer 1 with island thickenings (left and middle patterns) delineate the layers of (Nb)-solid solution and the intermetallic compound $Nb_5(Si,B)_3$. Their composition – $Nb_{80,0}(B_{10,6}Si_{9,4})_{20,0}$ (at.%) – is not identified with any of the intermetallic compounds. Focusing on the fact that after all, the boron concentration in the interlayer is larger than that of silicon, and then guided by the Nb–B diagram, it can be assumed that their composition belongs to the hypereutectic structure (Nb) + $Nb_3(B,Si)_2$. This phase composition corresponds to layers analogous to the classification after the first stage of welding in Figure 16*b*.
2. Oval regions (see the middle figure) contained diffuse formations of $Nb_3(B,Si)_2$ – Si-solid solution in Nb_3B_2, identified as an intermetallic compound of composition $Nb_{2,80}(B_{1,96}Si_{0,24})_{2,20}$. They are darker in color and, hence, lighter than the matrix phase of $Nb_5(Si,B)_3$.
3. On the left and right drawings, the white contours indicate the detection regions of the Nb(B,Si) phase of the Si-solid solution (up to 1.6 at.%) in boride NbB: $Nb_{0.86}(B_{1.10}Si_{0.03})_{1.14}$.
4. The right figure shows the localization of dark gray islet inclusions of the $Nb(Si,B)_2$ phase. Their average composition $Nb_{32.5}(Si_{64.4}B_{3.1})_{67.5}$ (at.%) corresponded to the stoichiometric formula $Nb_{0.98}(Si_{1.93B0.09})_{2.02}$.

The change in the phase structure of the main structural components of the composite with increasing time of DW and pressure can be summarized as follows.

1. Evolution of the layers that inherited the Nb-foil: [(Nb) + $Nb_3(B,Si)_2$] → [(Nb) with an Si concentration from 0 to 0.4 at.%] and the evolution of thin layers that demarcate them and diffusion SW: [Nb_3B_4 with a small concentration of Si] → [(Nb) + $Nb_3(B,Si)_2$].
2. Evolution of the outer layers of the interaction zone: [$Nb_3(B,Si)_4$] → [$Nb_5(Si,B)_3$] and the evolution of the mean of the ZI: [$Nb(Si,B)_2$ with boron to 2 at.% + NbB_2] → [$Nb(Si,B)_2$ with a low boron concentration + Nb(B,Si) with a small concentration of Si].

4.3. Heat resistant coatings

Experiments have been carried out to evaluate the possibility of obtaining protective heat-resistant coatings of molybdenum and tungsten silicides on the surface of a heat-resistant composite, in conjunction with the diffusion welding of a multi-layer package. A suspension coating of a mixture of Mo, W, and Si powders composed of 44 %Mo–44 %W–12 wt.%Si corresponding to one of the Novotny phases was applied to the outer Nb surfaces of the 4-Nb/(Si–B) packet, which was assembled from the elements with (Si–B)-coverings. It was assumed that carbon would fall into the coating due to the CO atmosphere in the welding chamber and ribbon spacers from the thermally exfoliated graphite (Sorokina, NE 2010) between the package and punches.

Figure 20 shows the coatings formed on the surface of the 4-Nb/(Si–B) composite after the 1st and 2nd stages of welding. Its thickness is ~ 60 μm. The study of the phase structure of the coating (Figure 21) after the first stage of the DW gave such results.

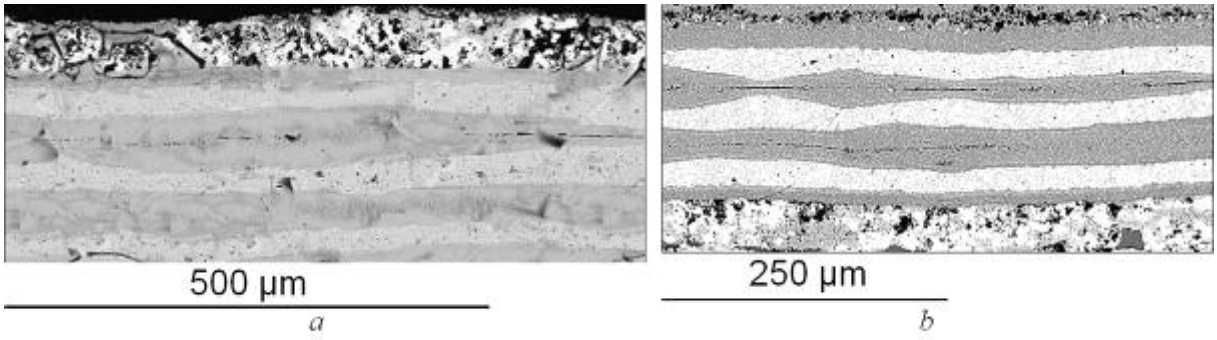


Fig. 20. Microstructure of the near-surface regions of the Nb/(Si–B) composite cross-section with coatings of molybdenum and tungsten compounds with silicon and carbon after the first (*a*) and the second (*b*) DW stages at 1500 °C

1. The composition of the coating revealed three phases:

– carbide-silicide Mo and W composition $(Mo_{30,36}W_{15,69})_{46,05}(Si_{27,71}C_{26,24})_{53,95}$ (at.%), which could be represented as equiatomic carbide-silicide compound (Mo,W)(Si,C) = $(Mo_{0.61}W_{0.31})_{0.92}(Si_{0.55}C_{0.53})_{1.08}$;

– molybdenum carbide-silicide with tungsten and niobium dissolved in it to 3 at% composition $(Mo_{37.76}W_{2.26}Nb_{0.59})_{40.61}(Si_{34.80}C_{24.85})_{59.65}$ (at%), to which, if identified with known compounds, MoC monocarbide MoC – $(Mo_{0.76}Me_{0.06})_{0.82}(Si_{0.69}C_{0.49})_{1.18}$ = (Mo,Me)(Si,C), where Me is W and Nb, is closest to the others;

– unused in reaction tungsten (light phase).

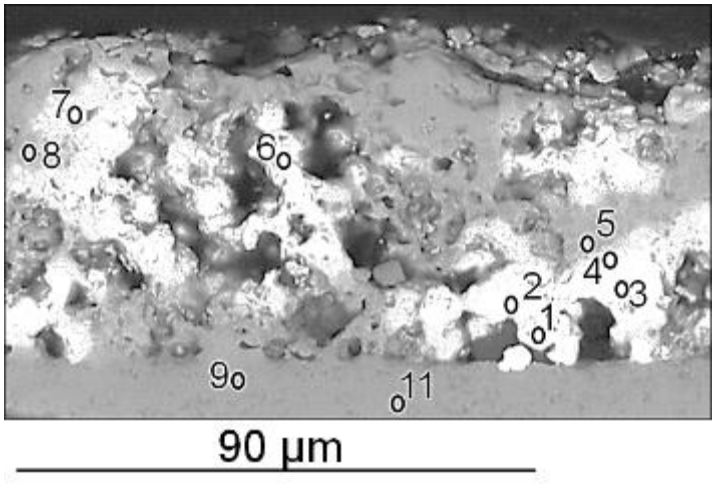


Fig. 21. Microstructure of the coating of molybdenum and tungsten compounds on the 4-Nb/(Si–B) composite after the 1st stage of the DW at 1500 °C for 1 *h*: 1–9, 11 – spectrum numbers

2. The composite layer adjacent to the coating (spectra 9 and 11) is the niobium monobarbide NbC_{1-x} with Mo, W and Si dissolved in it. Its composition $(Nb_{41.5}Me_{1.4})_{42.9}(C_{51.3}Si_{5.8})_{57.1}$ (at.%) is close to the monocarbide (Nb,Me)(C,Si)$_{1-x}$ = = $(Nb_{0.8}3Me_{0.03})_{0.86}(C_{1.03}Si_{0.11})_{1.14}$, where Me is Mo and W.

Conclusion. In the case of diffusion welding, 1500 °C for 1 hour, Novotny's phase of none of the known stoichiometric compositions $(Mo,W)_5Si_3C$ or $(Mo,W)_5Si_2$, for which the experiment was conducted, has not yet formed most likely, due to the low welding temperature. At the same time, the experiment showed that the diffusion interaction between such refractory elements as molybdenum, tungsten and carbon with silicon occurs quite actively, and will continue.

5. CHARACTERISTICS OF HEAT RESISTANCE, DENSITY AND MODULUS OF ELASTICITY OF COMPOSITES. MEASUREMENT OF THE CHARACTERISTICS OF HEAT RESISTANCE. TESTS AND CHARACTERISTICS OF THE DESTRUCTION OF COMPOSITES BASED ON MOLYBDENUM AND NIOBIUM

From the composites in the form of plates, samples were cut in the form of rods of rectangular cross section of 1–3 × 2–4 *mm* and a length of up to 40–60 *mm*, depending on the type of experiment. If fracture resistance tests were assumed, a lateral incision was made in the middle of the sample to a depth approximately to the middle of the cross section of the sample. Density, modulus of elasticity, strength, effective surface energy were also determined. The results of the tests showed an insignificant difference in the strength of two composites with molybdenum, in contrast to the noticeable differences in their structures. The strength was determined in the temperature range 20–1300 °C. The remaining measurements were carried out at room temperature. Since the material is structurally anisotropic, it was useful to test the strength, fracture resistance, and effective surface energy with loads applied perpendicularly and parallel to the layers of the structure under "three-point bending" conditions.

The fracture toughness was determined by calculating the critical stress intensity factor K^* under the conditions of planar deformation by the formula: $K^* = (P \cdot S/t \cdot h^{3/2}) \cdot f(a/h)$ (Broek, D 1980), where P is the maximum load, S is the distance between supports, t and h are the thickness and height of the sample, and a is the value of the lateral notch along the vertical. Tests of Nb/(Si–B) composites on crack resistance and on 3-point bending at room temperature were made with a perpendicular (⊥) and parallel (||) application of the load with respect to the surface of the layers.

High-temperature tests of composite samples for bending were carried out up to 1500 °C in an argon atmosphere at an excess pressure, somewhat above atmospheric pressure. The temperature was created by a multilayer heater made of niobium tapes 0.3 *mm* thick.

The density was determined by the standard method of hydrostatic weighing.

The modulus of elasticity E was calculated from the measurements of the resonant frequencies of the transverse oscillations of the sample in the form of a beam with a rectangular cross section constant in length. With oscillations, the samples bent in a plane perpendicular to the layers of the composite. The values of the modules were calculated by the formula: $E = 48 \cdot \pi^2 f^2 l^4 \rho / 3.52 \cdot h^2$ (Feodosev, VI 1979), where f is the resonance frequency of the transverse oscillations, l is half the length of the sample, h is the sample height, ρ is the density.

The anisotropy of the structure of the material led to a difference in the fracture toughness values of K^*. For composite samples based on molybdenum, it was 12.0 ± 6.0 and 14.0 ± 2.3 $MPa \cdot m^{1/2}$ when the load is applied perpendicularly (⊥) and parallel (||) to the layers of the structure, respectively. For composites based on niobium, 12.0 ± 0.5 and 13.0 ± 1.3 $MPa \cdot m^{1/2}$, respectively. Numerical values of crack resistance showed that both materials occupy an intermediate position between traditional ceramics and high-strength metal alloys.

Measurements of the density and modulus of elasticity are summarized in Table 3. For comparison, these properties (they were determined much earlier) are also presented for the (Ni–Al) -composite obtained by diffusion welding of Ni/Al-packets.

The formation of intermetallic compounds in the structure of composites led to a significant decrease in their density in comparison with the base metals: Nb (8570 kg/m^3), Mo (10200 *kg/m3*). The density of the composite with niobium proved to be even lower than that of Ni–Al.

The material	Ni/Al	1-Mo/(Si–B)	3-Nb/(Si–B)
Density, kg/m^3	7,5	8600	7200
Modulus of elasticity, *GPa*	220	270	130
Strength, *MPa*	–	620	600
Crack resistance, $MPa \cdot m^{1/2}$	–	12.0	13.0
Effective surface energy, J/m^2	–	10000	8000

Table 3. Characteristics of composite materials at room temperature (average values are given for 3–4 measurements). The test loads were applied perpendicular to the layers of the structure

The strengths σ_B when applied in directions perpendicular to and parallel to the plane of the layers, for example, for 3-Nb/(Si–B) were equal to $\sigma_{B\perp}$ = (600 ± 180) *MPa* and $\sigma_{B\parallel}$ = (790 ± 48) *MPa*, respectively. The higher strength $\sigma_{B\parallel}$ can be explained by the higher moment of resistance of high-modulus and high-strength boride-silicide layers in the direction parallel to that perpendicular to the layers.

In Figure 22 shows the results of short-term tests on 3-point bending of 3-Nb/(Si–B), 1-, and 2-Mo/(Si–B) composites at temperatures in the range of 1100-1500 °C. The $\sigma_B(T)$ dependence is significant in that the values of the strength of the order of 250 *MPa*, which are satisfactory for such temperatures, remain in the entire high-temperature interval.

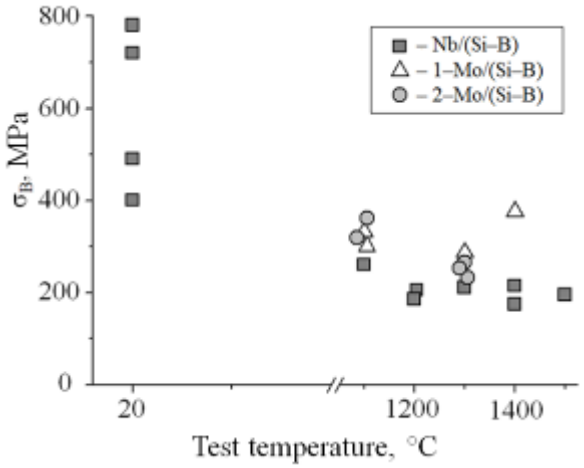


Fig. 22. Dependence of the strength σ_B of the Nb/(Si–B) and Mo/(Si–B) composites on the test temperature at the ⊥-application of loads with respect to the surface of the layers

The shape of the experimental deformation curves of composite samples with molybdenum (Figure 23) and niobium (Figure 24) indicates that their behavior under load when applied perpendicularly and parallel to the layers of the structure is significantly different. When the load is applied perpendicular to the layers, the curves have a nonlinear-step appearance, reflecting its local "jumps". Such features of deformation curves are characteristic of objects with non-fragile destruction, which is characterized by a change in the dominant types of micro-fracture when the macro-crack moves in the bulk of the sample.

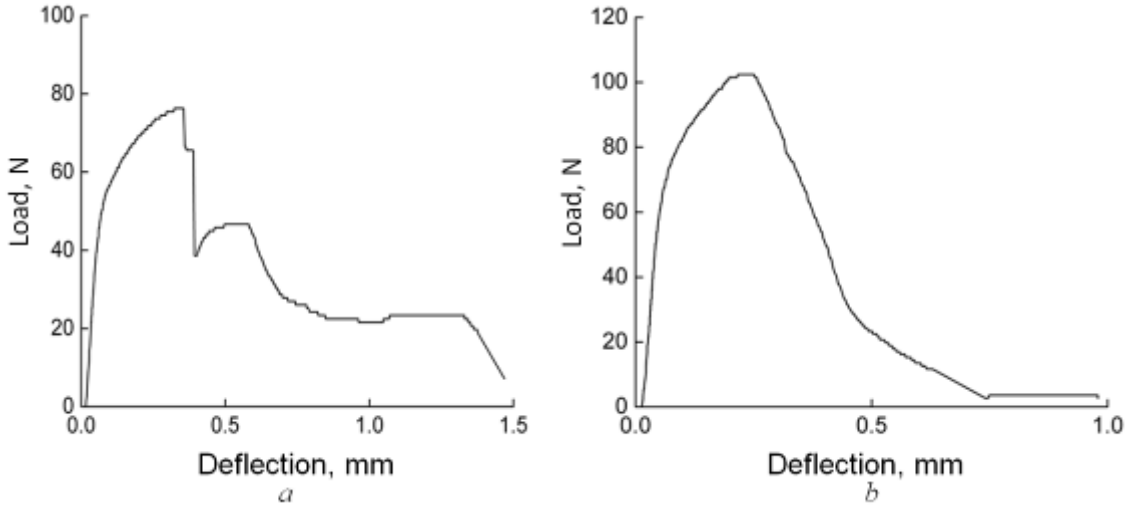


Fig. 23. Experimental load-deflection curves for 1-Mo/(Si–B) composites when the load is applied perpendicular to (*a*) and parallel to (*b*) the layers of the structure

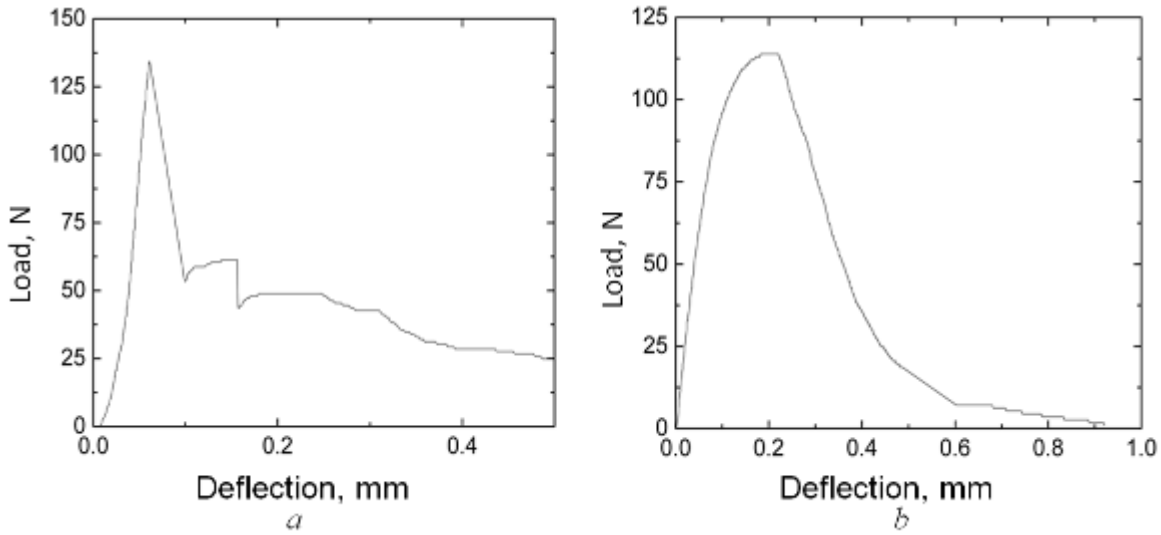
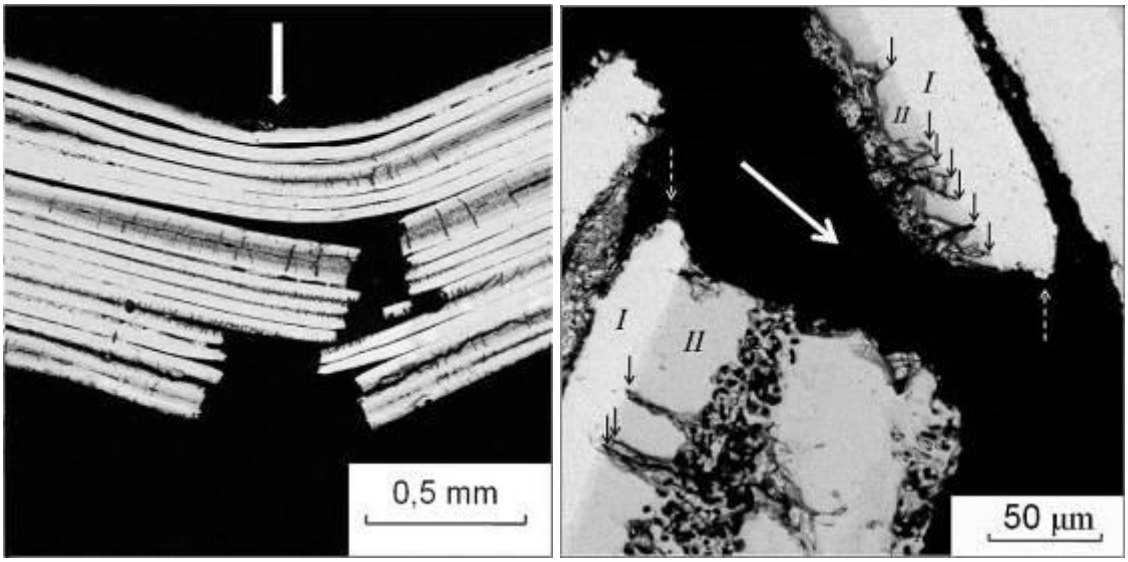


Fig. 24. Experimental load-deflection curves for 3-Nb/(Si–B) composites when the load is applied perpendicular to (*a*) and parallel to (*b*) the layers of the structure

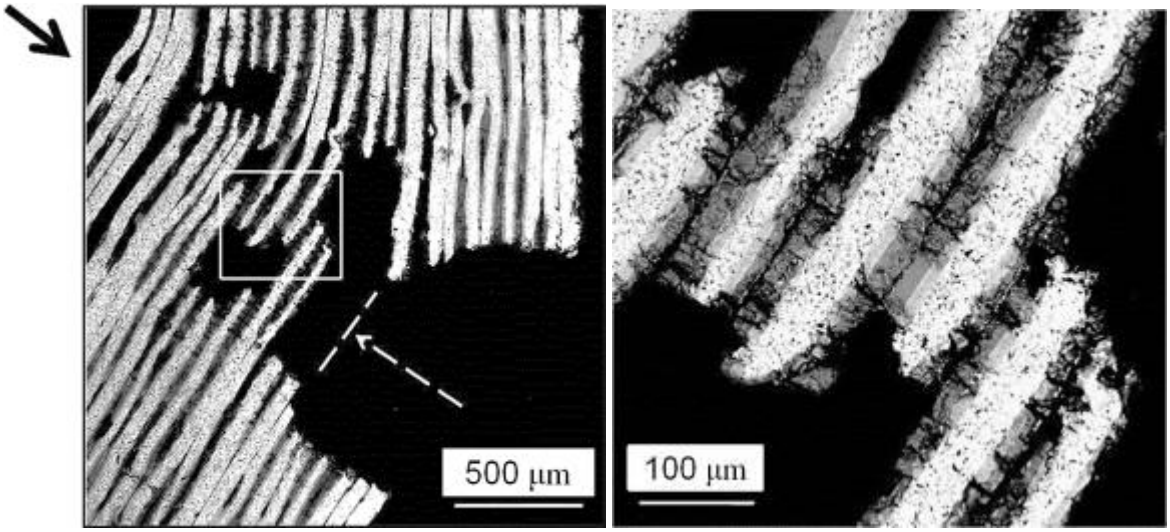
On microphotographs of the places of destruction, this can be evidenced by the tortuosity of the macrocrack trajectory (Figures 25*a* and 26*a*) and cleaving along the interfaces (Figure 27). Moreover, due to non-brittle fracture, the surface of the foliation is most often irregular and with ledges (inset in Figure 27*a*). Cleavages significantly affect the promotion of macrocracks in the body of the sample, changing its trajectory.

In addition to cleavages, a lot of cracking of brittle intermetallic phases (Figure 25*b*) and numerous "neck formation" in the layers of viscous-plastic solid solutions also occur during fracture (Figure 26*b*). Especially it is necessary to note the inhibition of microcracks on their boundaries with solid solutions (Figures 25*b* and 26*b*). All these types of microdisplays make a significant contribution to the energy absorbed by the material during destruction.



a *b*

Fig. 25. Macro- (*a*) and microstructure (*b*) of the cross-section of the 1-Mo/(Si–B) composite specimen without incision at the point of failure after flexural strength tests perpendicular to the layers of the structure: I – Mo-solid solution layers; II – layers of intermetallic compounds; black arrows – microcracks in intermetallic layers, dashed arrows – formation of "necks" in layers of Mo-solid solution



a *b*

Fig. 26. Macrostructure cross-sections of the composite sample 3-Nb/(Si–C) after a short (for 30 min at 1400 C) welding with a notch after failure in flexural strength tests perpendicular to the layers of the structure (*a*) and the microstructure of the selected area in the left figure (*b*): black arrow – load application; the dotted arrow indicates the depth of the incision.

The remark to Figbre 26b. The light layers associated with the structural component based on the Nb alloy (shown by arrows) have fine dispersions of gray and dark color (Figure 27). With the help of local X-ray spectral analysis it was established that the first are niobium carbosilicide $(Nb,Me)_2(C,Si)$, where Me is Ti, Cr, Al and Fe, the second is TiC carbide.

When the load is applied parallel to the layers of the structure, the nonlinearity of the experimental curves is also present, but it is smoothed out and has a steeper decrease (Figures 23*b* and 24*b*) than for the perpendicular orientation of the load application direction with respect to the layers. This is determined by the simpler mechanisms of destruction during the passage of the macro-crack along the structural layers. However, some foliations are observed here (Figure 27*b*), as well as the formation of a small number of microcracks in the layers of intermetallic phases (Figure 28). The main contribution to the fracture toughness also in this case is the plastic deformation of the layers of a solid solution of silicon and boron in molybdenum and niobium.

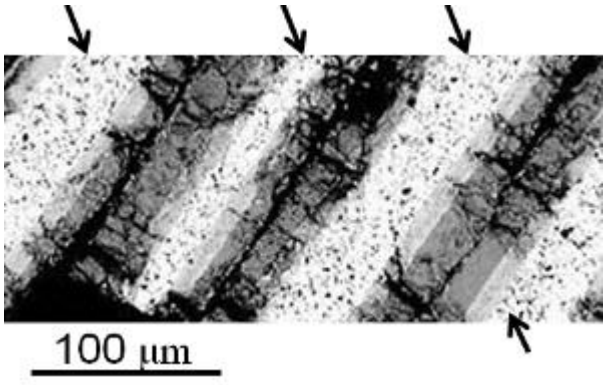
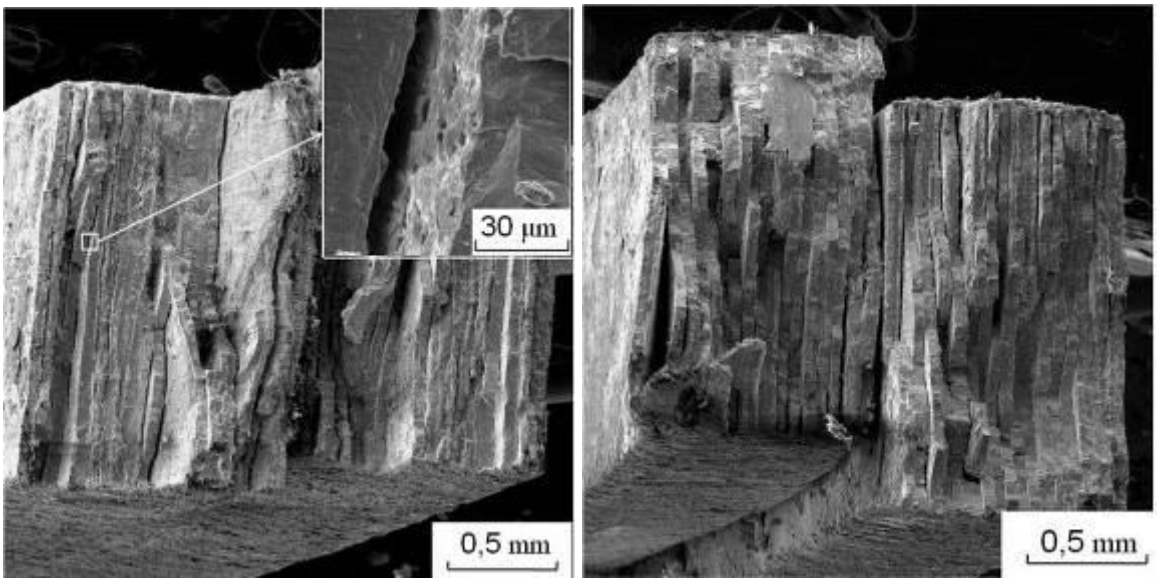
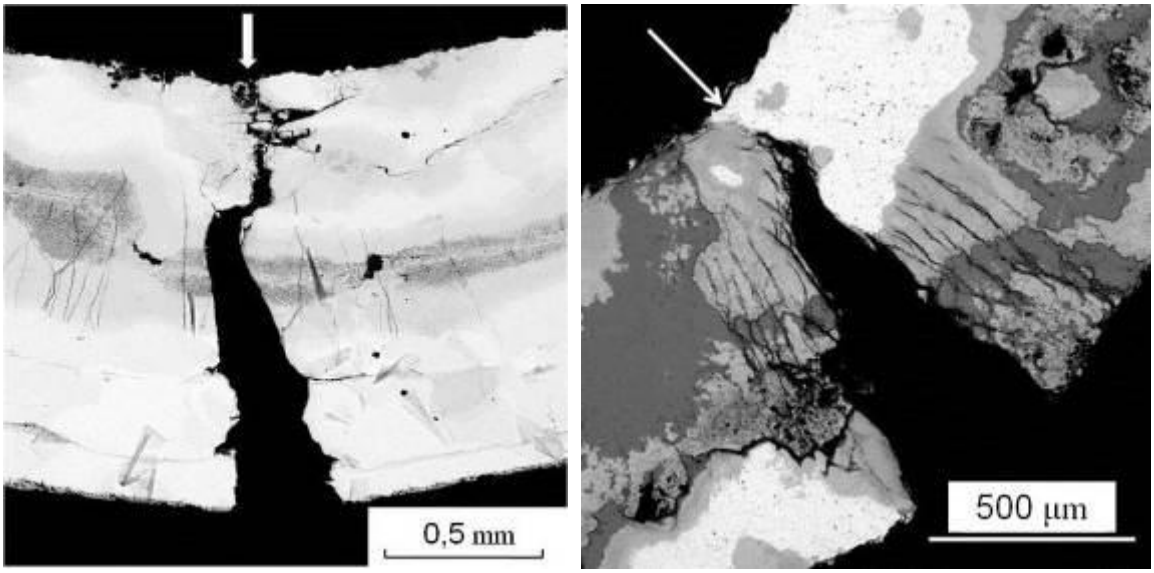


Fig. 27. To the remark on Figure 26*b*



a *b*

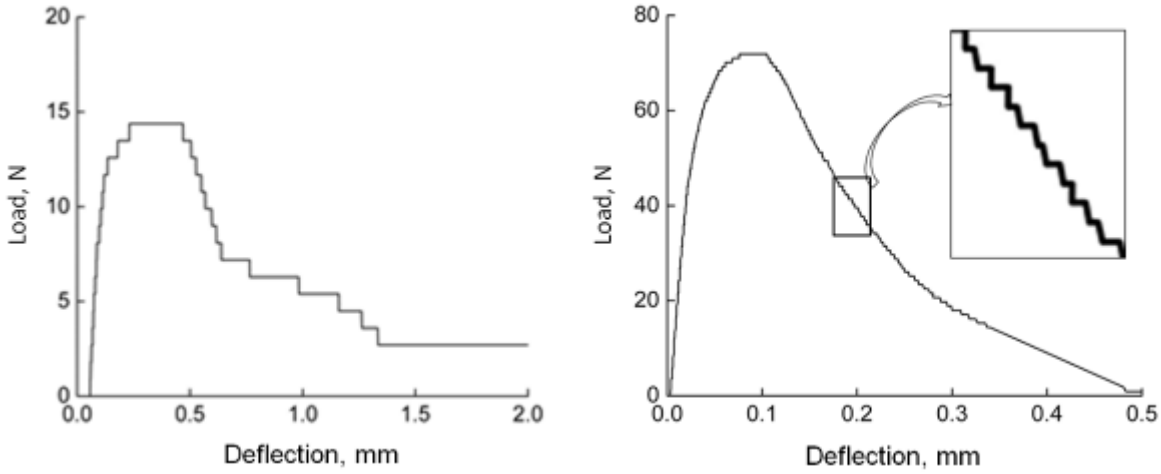
Fig. 28. Surfaces of fracture of 1-Mo/(Si-B) samples in strength tests with by applying the load perpendicularly (*a*) and parallel (*b*) to the layers of the structure



a *b*

Fig. 29. Sections of the samples in a plane parallel to the layers, after the destruction (arrows indicate the directions of application of the loads): *a* – 1-Mo/(Si–B); *b* – 3-Nb/(Si–C)

From the ones shown in Figure 30 dependences of the deflection from the applied load in two directions relative to the surface of the layers when testing for the fracture toughness of composite samples with molybdenum, one can see that their appearance differs from the same curves for specimens without cuts by a set of well-defined "ledges" reflecting the discrete advance of the crack in the volume of the layered composite. It can be assumed that for a perpendicular orientation of the direction of application of the load and the layers, the ledges have a macroscopic scale, and for parallel orientation the microscopic orientation (see the inset in Figure 30*b*).



a *b*

Fig. 30. Experimental dependences of the load-deflection of specimens with incisions from the 2-Mo/(Si–B) composite after tests for crack resistance with a load applied perpendicularly (*a*) and parallel to (*b*) layers of the structure

Destruction of the samples during the strength tests can be considered as dividing them into two parts by a macroscopic crack that has passed in the transverse direction through the sample and the

formation of two new surfaces (failure surfaces). An estimate of the effective surface energy of failure g in this case can be defined as the ratio of the work of external forces in breaking a sample to twice the area of its cross section:

$$g = (1/2F)\int_x Q(x)dx ,$$

where Q – the load on the sample, x – the movement of the point of application of the load to the sample or the deflection of the sample, F – the cross-sectional area of the sample. For an example, let us estimate the effective surface energy of Mo/(Si–B) composites. In reality, this is the area under the experimental load-deflection curve.

The calculated values of g, if the load was applied perpendicularly and parallel to the layers of the structure (Figure 30), were 10×10^3 and 6.3×10^3 J/m^2, respectively. Contribution to the work of destruction during the passage of the macrocrack is made:

– the effective surface energy of the components of the structure, which in our case are solid solutions, intermetallic compounds and boride-silicides,

– surface energy of microcracks,

– foliations deformation of non-brittle layers of solid solutions,

– bundles along the interfaces of the components and

– friction on the formed surfaces of microfractures.

The difference in the values of the effective surface energy when the load is applied perpendicularly and parallel to the plane of the layers of the structure of composites is explained by the involvement of various types of microfractures in the overall destruction and in their number when the macrocrack passes perpendicularly or parallel to the layers.

6. CONCLUSIONS

At this stage of the study, we can draw the following conclusions and conclusions on the layered composites based on molybdenum and niobium with boride-silicide hardening, obtained by solid-phase method.

1. It has been established that molybdenum and niobium readily enter into solid-phase interaction with powdered boron-silicon coatings if they are brought into tight contact in an artificially assembled package, which is essentially a multilayered set of diffusion pairs, and it is manageable to act on the package with temperature and pressure.
2. The resulting layered composites are sufficiently complete and reliably studied by scanning electron microscopy and X-ray spectral analysis. Spectral analysis in comparison with the corresponding state diagrams at the current stage of research is the main tool for identifying the phase structure of composites. The object is open for research by other modern methods.
3. It has been shown that it is possible to purposefully influence the phase composition of the layered structure of composites by varying the thickness and varying the composition of the metal strips and coatings (1) and changing the temperature and time of the diffusion welding of the packets (2).
4. Almost all the methods we need to measure the density, modulus of elasticity, high-temperature strength, crack resistance and effective surface energy have been tested for the Mo/(Si–B) and Nb/(Si–B) composites.
5. The strength of the Mo/(Si–B) and Nb/(Si–B) composites obtained is not inferior to the best structural alloys of a similar design in a wide range of temperatures, and exceeds many of them in rigidity. The crack resistance of the composites obtained, occupying an intermediate position

between ceramics and high-strength alloys, is not yet quite sufficient. The composite structure needs to be optimized by selecting the initial compositions and technological regimes.

6. The obtained results on structure formation, mechanical testing and analysis of fracture processes are quite general in nature and can serve as a basis for the development of other layered structural materials based on refractory metals strengthened by intermetallic compounds.
7. The "pilot" experiment on the formation of a heat-resistant coating of tungsten and molybdenum compounds on the surface of a Nb/(Si–B) composite at the same time as a heat-resistant layered structure is evidence of the broader possibilities of the solid-phase technology being developed.

ACKNOWLEDGMENT

The work was supported by the Russian Foundation for Basic Research (project No. 17-03-00687 A).

REFERENCES

1. Kosolapova, TYu 1986, Properties, production and application of refractory compounds. / Ed. T.Ya. Kosolapova, Moscow: Metallurgy. – 928 p.
2. Schneibëel, JH 2003, "High temperature strength of Mo–Mo_3Si–Mo_5SiB_2 molybdenum silicides". *Intermetallics*, no 11, pp. 625–632.
3. Sharif, AA 2005, "Strength of $MoSi_2$-based crystals at ultra-high temperature". Sharif A.A., Misra A., Mitchell T.E. *Scripta Materialia*, no 52, pp. 399–402.
4. Jain, P 2010, "Tensile Creep of Mo–Si–B Alloys", Kumaru K.S. *Acta Materialia*, v. 58, no 6, pp. 2124–2142.
5. Goronovsky, IT 1987, "Quick reference book on chemistry". I.T. Goronovsky, Yu.P. Nazarenko, E.F. Nekryach, Kiev: Naukova Dumka. – 929 p.
6. Cook, J 1964, *Proceedings of the Royal Society*, Cook J., Gordon J.E., v. 282, no 8, pp. 508.
7. Anishenkov, VM 1978, "Fatigue destruction of a layered composite". Anishenkov V.M., Mileiko S.T. *DAN SSSR*, v. 241, no. 5, pp. 1068–1069.
8. Kolchin, AA 2001, "Oxide/oxide composites with fibres produced by using internal crystallization method". Kolchin A.A, Kiiko V.M., Sarkissyan N.S., Mileiko S.T. *Composite Science and Technology*, v. 61, no 7, pp. 1079–1082.
9. Pouchou, JL 1984, "A new model for quantitative X-ray microanalysis. I. Application to the analysis of homogeneous samples". Pouchou J.L., Pichoir F. *Recherche Aerospatial*, v. 3, pp. 13–38.
10. Sorokina, NE 2010, Composite nanomaterials based on intercalated graphite. Textbook for students on the specialty "Composite nanomaterials". N.E. Sorokina, V.V. Avdeev, A.S. Tikhomirov, M.A. Lutfullin, M.I. Saidaminov, Moscow: Moscow State University. M.V. Lomonosov – 50 p.
11. Broek, D 1980, Fundamentals of fracture mechanics. D. Broek, Moscow: Высшая школа, – 368p.
12. Feodosev, VI 1979, Strength of materials. V.I. Feodosev, Moscow: Наука, – 560 p.